Applied Surface Science xxx (2014) xxx–xxx

Contents lists available at ScienceDirect

Applied Surface Science

journal homepage: www.elsevier.com/locate/apsusc

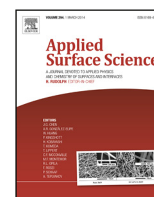

Controlled synthesis of transition metal dichalcogenide thin films for electronic applications

Riley Gatensby [a,b], Niall McEvoy [a], Kangho Lee [a], Toby Hallam [a], Nina C. Berner [a], Ehsan Rezvani [a,b], Sinéad Winters [a,b], Maria O'Brien [a,b], Georg S. Duesberg [a,b,*]

[a] Centre for Research on Adaptive Nanostructures and Nanodevices (CRANN), Trinity College Dublin, Dublin 2, Ireland
[b] School of Chemistry, Trinity College Dublin, Dublin 2, Ireland

ARTICLE INFO

Article history:
Received 6 December 2013
Received in revised form 15 January 2014
Accepted 16 January 2014
Available online xxx

Keywords:
2D materials
Transition metal dichalcogenides
Nanoelectronics
Sensors
Spectroscopy
Thin films

ABSTRACT

Two dimensional transition metal dichalcogenides (TMDs) are exciting materials for future applications in nanoelectronics, nanophotonics and sensing. In particular, sulfides and selenides of molybdenum (Mo) and tungsten (W) have attracted interest as they possess a band gap, which is important for integration into electronic device structures. However, the low throughput synthesis of high quality TMD thin films has thus far hindered the development of devices, and so a scalable method is required to fully exploit their exceptional properties. Within this work a facile route to the manufacture of devices from MoS_2 and WS_2, grown by vapour phase sulfurisation of pre-deposited metal layers, is presented. Highly homogenous TMD films are produced over large areas. Fine control over TMD film thickness, down to a few layers, is achieved by modifying the thickness of the pre-deposited metal layer. The films are characterised by Raman spectroscopy, electron microscopy and X-ray photoelectron spectroscopy. The thinnest films exhibit photoluminescence, as predicted for monolayer MoS_2 films, due to confinement in two dimensions. By using shadow mask lithography, films with well-defined geometries were produced and subsequently integrated with standard microprocessing process flows and electrically characterised. In this way, MoS_2 based sensors were produced, displaying sensitivity to NH_3 down to 400 ppb. Our device manufacture is versatile, and is adaptable for future nanoscale (opto-) electronic devices as it is reproducible, cost effective and scalable up to wafer scale.

© 2014 Elsevier B.V. All rights reserved.

1. Introduction

The novel properties of two dimensional semiconducting transition metal dichalcogenides (TMDs) make them of great interest for both academia and industry [1–3]. They offer an exciting alternative to graphene, as they possess a band gap, which is crucial for applications in electronics and photonics. These materials have the general formula MX_2 with M being a transition metal (commonly, but not limited to, Mo, W, Nb, Ta, Ti); and X being a chalcogen (S, Se, Te). This class can form two-dimensional layered films composed of a plane of metal atoms covalently bonded to chalcogen atoms. Bulk crystals of such materials have long been studied[4], but in recent years the isolation of their 2D analogues has led to renewed interest in this field.

Importantly, a transition from an indirect gap to a direct gap semiconductor has been reported for MoS_2 [5], and WS_2 [6,7] as they approach monolayer thickness. Single layer MoS_2 shows a transition from the bulk indirect band gap of 1.2 eV, to a direct band gap of 1.9 eV [8]. The WS_2 analogue shows a similar transition with a bulk indirect band gap and monolayer direct band gap of 1.4 eV and 1.8 eV, respectively [9]. Recent work has used micromechanically exfoliated layers to produce devices which demonstrate excellent on/off ratios and rapid switching [10–12]. Layers exfoliated by this method have been shown to display photoluminescence (PL) [13] and electroluminescence [14], and thus have potential applicability in optoelectronic devices. However, this production method is very laborious and offers no prospect of scalability.

Scalable production of 2D TMDs has recently been achieved using sonication assisted liquid phase exfoliation in organic solvents [15] and surfactant media [16] as well as by Li intercalation [17,18] and by thermal decomposition of tetrathiomolybdates (or tetrathiotungstates) [19]. Such methods can be used to produce bulk quantities, well suited for applications in composites [20–23], catalysis [19], lithium ion batteries [24,25] and supercapacitors

* Corresponding author at: Centre for Research on Adaptive Nanostructures and Nanodevices (CRANN), Trinity College Dublin, Dublin 2, Ireland.
E-mail address: duesberg@tcd.ie (G.S. Duesberg).

http://dx.doi.org/10.1016/j.apsusc.2014.01.103
0169-4332/© 2014 Elsevier B.V. All rights reserved.

[26]. However, they are not readily compatible with standard microprocessing techniques; and the films produced from individual flakes display inferior electronic properties to those obtained by mechanical exfoliation [27]. Chemical vapour deposition (CVD) is a versatile, cost effective and industry compatible technique, which has greatly advanced graphene research in recent years by making high quality films readily available [28,29]. Similar methods can be used for the production of TMD films, and several routes to the production of MoS_2 thin films have recently been outlined. These typically are not pure CVD processes but rather involve thermally assisted sulfurisation of Mo [30–32] or, more commonly, MoO_3 [33–36], however the use of liquid phase precursors has also been demonstrated [37,38]. WS_2 has similarly been produced through the thermally assisted sulfurisation of WO_3 [33] and W [39] or by atomic layer deposition [40]. However, fine control of TMD layer thickness over large areas, in combination with structured growth, has seldom been demonstrated.

Within this work a facile route to manufacture of devices from TMDs, grown by vapour phase sulfurisation, is presented. Highly homogenous TMD films are produced over large areas by sulfurisation of pre-deposited metal layers. This is demonstrated for MoS_2 and WS_2, but can potentially be extended to produce other TMDs. The thickness of the samples is well controlled, from bulk down to monolayer, and high quality homogenous films are produced over a centimetre scale. The uniformity of these films, as observed through scanning Raman analysis, signifies an advance on existing reports on the sulfurisation of Mo which typically show non-uniform films with limited thickness control [31]. By using shadow masks we obtain films with well-defined geometries that can be readily integrated with standard micro-processing technologies. This procedure minimises processing steps, and results in quick, cost effective and versatile device manufacture.

One area of application, which is highly technologically relevant, is chemical sensors. The ever increasing demand for highly sensitive, low cost and low power sensors, in particular for standalone and mobile systems, has necessitated the investigation of new materials. Electronic gas sensors, based on 1D and 2D nanomaterials in a field effect transistor (FET) configuration, have shown considerable promise [41–43]. Improvements in their sensitivity and selectivity have continuously been demonstrated through covalent or non-covalent functionalisation [44–46]. As a semiconducting analogue of graphene, which has demonstrated single molecule detection [43], 2D MoS_2 is an exciting candidate for future sensors. A number of MoS_2 based gas sensors have recently been reported using micromechanically exfoliated [11,47,48] and liquid phase exfoliated [49,50] MoS_2 flakes. However, these approaches suffer from the previously mentioned problems of poor scalability and poor electronic quality, respectively and it is only recently that devices from more scalable processes have been reported [51]. In this study, we show that our simple process flow is capable of producing gas sensing devices with ultra-high sensitivities, down to 400 ppb for ammonia.

2. Experimental

Thin metal films (Mo, W, 99.99% MaTecK) were sputtered onto substrates (300 nm SiO_2 on Si and fused quartz, Alfa Aesar) using a Gatan Precision Etching Coating System (PECS) allowing for variable thicknesses (0.5–20 nm). The film deposition rate, and thickness, was monitored using a quartz crystal microbalance, maintaining a deposition rate of <0.1 nm/s. Hard masks were used to pattern the coatings, thus defining selective areas of film growth.

Substrates were placed in a quartz tube furnace (Lindberg Blue) and heated (~50 °C/min) to 500 °C under Ar flow (150 sccm, $P \sim 0.7$ Torr). After a 5 min dwell at 500 °C, the samples were heated to 750 °C (25 °C/min) and annealed for 30 min. A second upstream hot zone was used to melt S powder (MaTecK, 99%) to 113 ± 0.1 °C, and thus introduce S vapour into the reaction zone. This hot zone consisted of an assembly of halogen bulbs coupled with a power supply. A k-type thermocouple, placed alongside the S supply, allowed for the temperature in the vicinity of the S powder to be monitored. Following sulfurisation, the samples were held at 750 °C for a further 20 min, before the furnace was cooled. Upon removal from the furnace, samples were cleaned with acetone and then isopropanol (both HPLC grade) to remove unreacted residue.

For deposition of metal leads a hard mask was aligned to the prestructured TMD films and Ti/Au (10/80 nm) was deposited with the Gatan PECS.

High resolution transmission electron microscopy (HRTEM) bright field images were obtained using a FEI Titan 80–300 TEM. Samples were prepared by first spin coating a PMMA support layer onto the MoS_2 thin films and then etching the substrate with 15 M KOH. Samples were then transferred to lacey carbon TEM grids and the PMMA removed by immersion in acetone.

Raman analysis was performed using a Witec Alpha 300R confocal Raman microscope, utilising a 532 nm laser and an 1800 lines/mm grating. A laser power of less than 1 mW was used for all measurements in order to avoid sample damage. Raman maps were obtained by taking 4 scans every μm in the *x* and *y* direction. PL measurements were taken using the same system with a 600 lines/mm grating in a high cm^{-1} regime.

X-ray photoelectron spectroscopy (XPS) was performed under ultra-high vacuum conditions (base pressure of 2×10^{-10} mbar) using a VG Scientific CLAM2 analyser operated at a pass energy of 50 eV with 2 mm slits, giving a FWHM on Ag $3d_{5/2}$ of 1.25 eV for the source (PSP twin anode, unmonochromatised Al K_α, operated at 12 kV and 12 mA). The core-levels were fitted using the software CasaXPS.

Electrical characteristics were measured under ambient conditions using a Karl Suss probe station in conjunction with a Keithley model 2612A source meter.

Gas Sensing measurements were performed in a homemade gas sensing chamber. 200 ppm NH_3 gas, balanced by dry N_2, was introduced into the chamber using mass flow controllers to dilute the gas concentration by mixing with dry N_2. At a 100 sccm flow of the NH_3/N_2 mixture, the gas sensing chamber was kept at a pressure of 10 Torr. The electrical resistance of MoS_2 sensors was measured using a Keithley model 2612A source meter at a constant bias voltage of 0.2 V and all measurements were performed at room temperature. In every test, the MoS_2 sensors were exposed to pure N_2 for 2 min to record their initial resistance and then NH_3 gas was introduced for 2 min, and the sensor response measured. The sensors were exposed to N_2 for 10 min to recover and the gas sensing tests were periodically repeated four times.

3. Results and discussion

TMD thin films were produced by direct sulfurisation of predeposited metal films in a quartz tube furnace with two heating zones. MoS_2 formed the primary focus of our study; however our method was also well-suited to the production of WS_2. Thin films of Mo (W) of nominal thicknesses, between 0.5 and 20 nm, were heated to a growth temperature of 750 °C and S powder was then melted in a second upstream heating zone. Using Ar as a carrier gas, S vapour was transported to the substrates, forming MoS_2 (WS_2) at predefined locations. A schematic of this process is shown in Fig. 1a. Films were grown on both SiO_2/Si and fused quartz substrates by sulfurisation of films with different thicknesses of pre-deposited metal. Photographs of MoS_2 films, on both SiO_2/Si

Please cite this article in press as: R. Gatensby, et al., Controlled synthesis of transition metal dichalcogenide thin films for electronic applications, Appl. Surf. Sci. (2014), http://dx.doi.org/10.1016/j.apsusc.2014.01.103

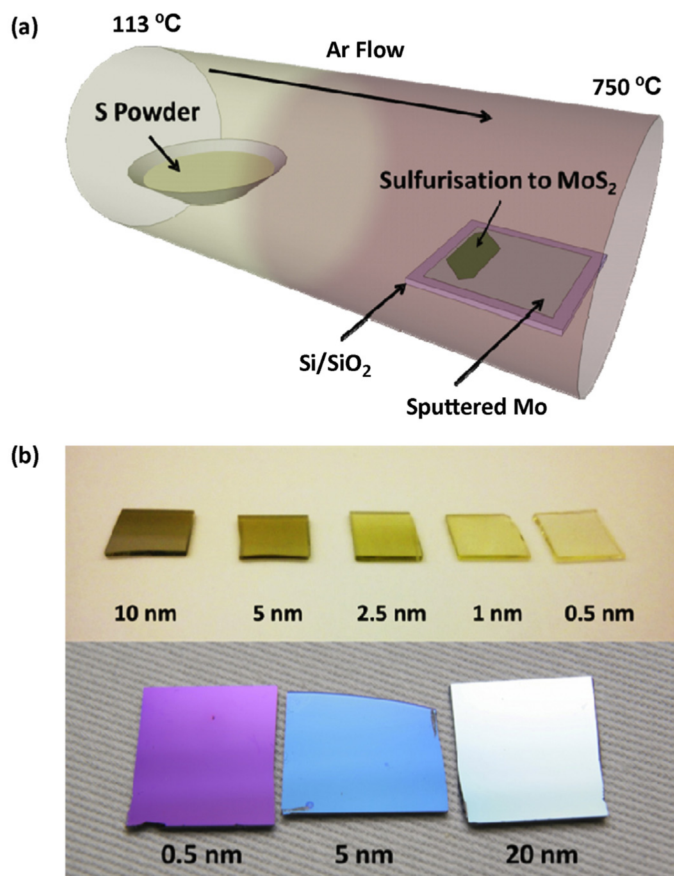

Fig. 1. (a) Schematic diagram of the sulfurisation of Mo. Two distinct heating zones were used; the growth substrates were held at 750 °C, while in a second upstream heating zone S powder was heated to 113 °C. (b) Photograph of MoS_2 films formed by sulfurisation of Mo films of different thickness on fused quartz (top) and SiO_2/Si (bottom) substrates. An increase in opacity with increasing starting film thickness is evident. Each sample shown has an area of ~1 cm^2.

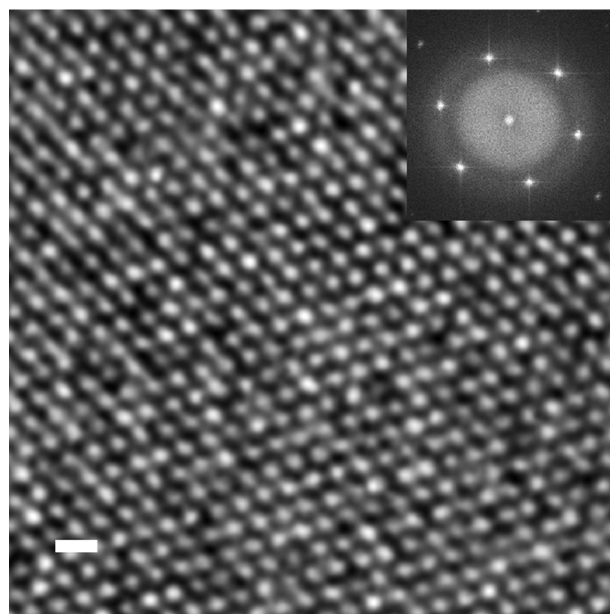

Fig. 2. HRTEM image of a typical MoS_2 thin film (nominal Mo thickness of 5 nm). Scale bar is 1 nm. Inset is a FFT of the enlarged image showing hexagonal symmetry; sharp spots confirm a very low level of defects.

and fused quartz, are shown in Fig. 1b. Films are easily distinguished from one another, even those with pre-deposited film thicknesses of 0.5 nm and 1 nm, indicating good control over film thickness. HRTEM was used to probe the crystalline quality of MoS_2 films. Films were transferred to grids by etching away the underlying Si substrate in 15 M KOH. An atomic resolution image of a typical thin film (5 nm Mo thickness) is shown in Fig. 2. It clearly shows the hexagonal lattice structure of the film suggesting it is highly crystalline MoS_2. The inset shows a fast Fourier transform (FFT) of the HRTEM image. The well-defined spots indicate a low level of

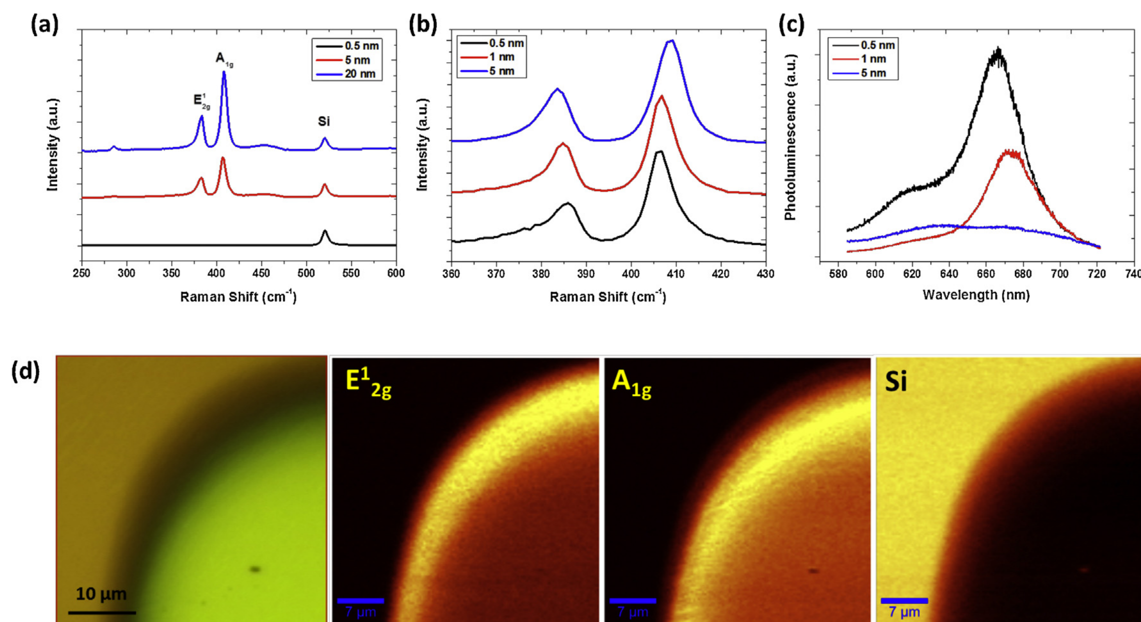

Fig. 3. (a) Raman spectra for three different MoS_2 film thicknesses normalised to the Si (520 cm^{-1}) peak intensity. (b) Raman spectra for three different MoS_2 film thicknesses normalised to the A_{1g} peak intensity highlighting the evolution of spectra with decreasing thickness. (c) PL spectra for the same films as (b), normalised to the Raman intensity, showing strong emission for the 0.5 nm film and none for the 5 nm film. (d) Optical image and scanning Raman maps of the , A_{1g} and Si peaks for a shadow mask patterned film of 10 nm starting thickness.

defects. There was some contamination on the surface of the films, most likely caused by the film transfer process, which involves a PMMA support layer and basic etchant, which could potentially be the cause of the background noise in the FFT. An intensity profile was extracted from the HRTEM image (see supporting information Fig. S1). From this profile, the d-spacing was measured to be 0.63 nm. This is in good agreement with the previously reported spacing of (0 0 2) planes of hexagonal MoS_2 [52].

Raman spectroscopy was used to assess the layer thickness and uniformity of our films. Bulk MoS_2 has two well-known Raman bands at 383 cm^{-1} and 407.8 cm^{-1} when probed with a 532 nm excitation laser [53]. These correspond to E^1_{2g} and A_{1g} vibrational modes, respectively. Spectra of three films, with different starting Mo thicknesses, grown on Si/SiO_2, are shown in Fig. 3a. It is clear that the relative intensity of the MoS_2 bands to the Si peak of the substrate at 520 cm^{-1} scales with increasing film thickness, confirming that the thickness of MoS_2 produced is directly related to the starting Mo thickness.

Li et al. described the evolution of the Raman signal of mechanically exfoliated MoS_2 flakes upon reducing the number of layers. They observed an upward shift of 1.7 cm^{-1} and a downward shift of 5.1 cm^{-1} in the and A_{1g} peaks, respectively, upon going from bulk crystals to monolayers[53]. Such a trend was previously predicted from *ab initio* calculations by Molina-Sánchez et al. [54]. Spectra of three films of different thickness, normalised to the A_{1g} peak intensity are shown in Fig. 3b. As expected, the E^1_{2g} and A_{1g} peaks shift closer to one another with decreasing film thickness. In the case of the 5 nm sample the and A_{1g} peaks are seen at 383.6 cm^{-1} and 408.6 cm^{-1}, a separation of 25 cm^{-1}, whereas for the 0.5 nm sample the same peaks manifest at 385.9 cm^{-1} and 406.3 cm^{-1}, a separation of 20.4 cm^{-1}. This suggests that the 0.5 nm sample consists of very few (1–3) layers, whereas the 5 nm sample behaves like bulk MoS_2. It is probable that the laser, with a spot size of ~300 nm, probes a number of crystal sites and thus the observed Raman

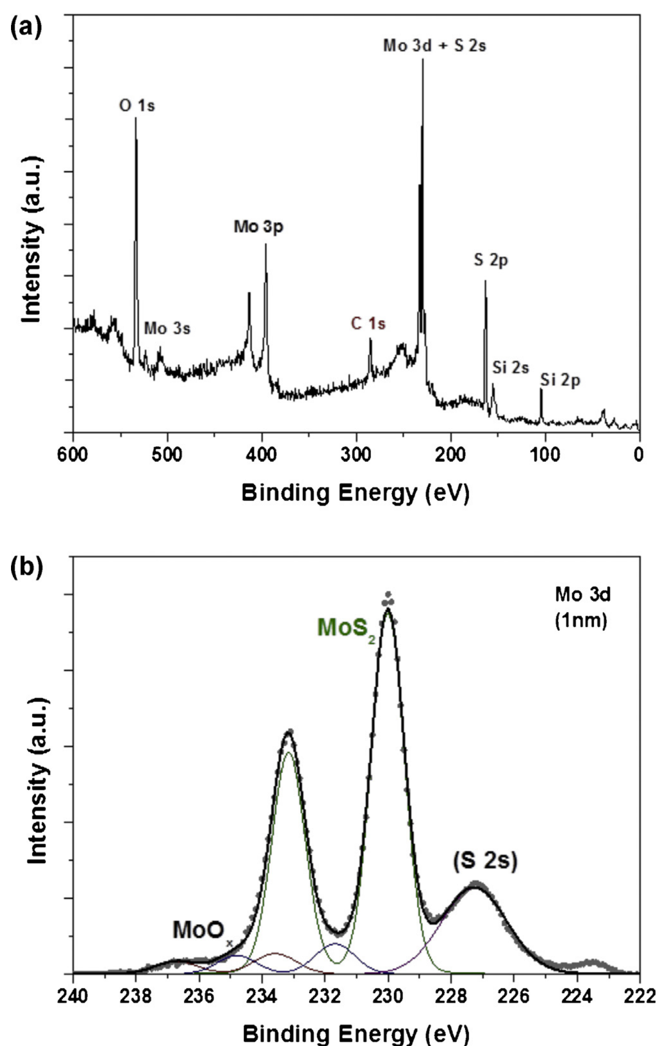

Fig. 4. (a) An XPS survey spectrum for a film with an initial Mo thickness of 1 nm. The difference in binding energy between the Mo $3d_{5/2}$ and the S $2p_{3/2}$ peaks of $\Delta E = 67.1$ eV indicates a stoichiometric ratio in our MoS_x samples of $x = 1.9 \pm 0.1$. The lack of major contaminants, except natural organic matter (C), is also evident. (b) The Mo 3d core-level with fitted components after subtraction of a Shirley background, also including the S 2s core-level in the same binding energy region. The main component at 230 eV corresponds to sulfurised Mo, with two minor components at 231.7 eV and 233.6 eV originating from residual oxides. The spin-orbit splitting in the Mo 3d doublets is 3.25 eV and the branching ratio (Mo $3d_{3/2}$ to Mo $3d_{5/2}$) is 2:3. All components of the Mo 3d line have been fitted using a mixed Gaussian–Lorentzian line shape with a FWHM of 1.3 ± 0.1 eV.

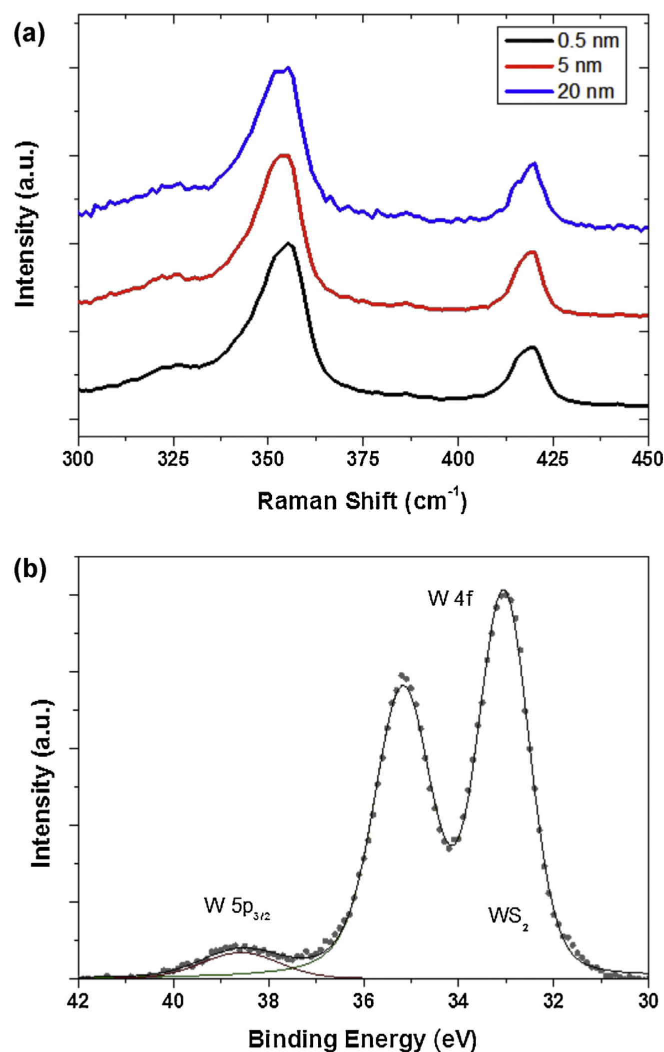

Fig. 5. (a) Raman spectra for three different WS_2 film thicknesses normalised to the A_{1g} peak intensity. Unlike the corresponding MoS_2 spectra, thickness dependent peak shifts are not immediately obvious. (b) XPS of the W 4f core-level of a WS_2 film with an initial W thickness of 20 nm, after subtraction of a Shirley background and with the W $5p_{3/2}$ line in the same binding energy range. The 4f line was fitted with a single component at a binding energy of 33.05 eV (for the $4f_{7/2}$), which indicates completely sulfurised W at the surface. The spin-orbit splitting in the W 3f doublet is 2.13 eV and the branching ratio (W $4f_{5/2}$ to Mo $4f_{7/2}$) is 3:4. The line has been fitted using a mixed Gaussian-Lorentzian line shape with a FWHM of 1.15 ± 0.10 eV.

Please cite this article in press as: R. Gatensby, et al., Controlled synthesis of transition metal dichalcogenide thin films for electronic applications, Appl. Surf. Sci. (2014), http://dx.doi.org/10.1016/j.apsusc.2014.01.103

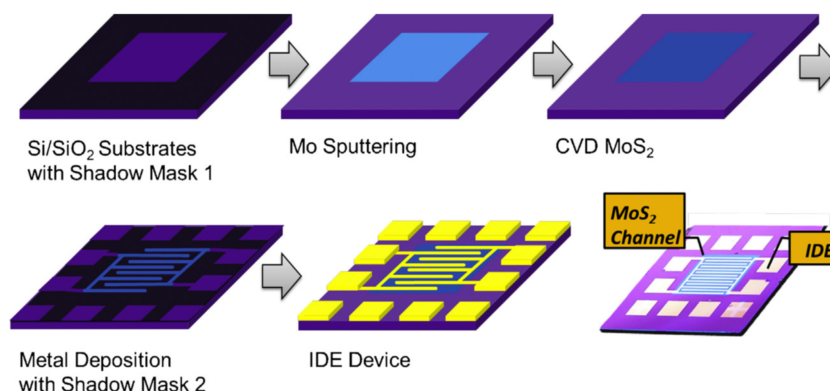

Fig. 6. Schematic representation of the process steps involved in producing a TMD channel device. Selective areas are defined with a shadow mask, metal is sputtered, the sample is sulfurised, IDE contacts are defined, and contacts are sputtered. The bottom right panel is a photograph of one such device, 1.5 cm × 1.5 cm in area. The dimensions of the channel are 5.4 mm × 5.4 mm. The interdigitated electrode (IDE) pattern used for the contacts has a channel length of 200 μm and a width of 5.54 cm (=277 × Length).

signal may consist of contributions from domains of different layer thickness.

PL studies offer an alternative route to probing the thickness, and electronic properties, of MoS_2 films. Splendiani et al. measured PL spectra for MoS_2 flakes of different thickness [5]. In bulk MoS_2, with its indirect band gap, they observed no PL emission. However, in few- and monolayer crystals they noted PL emissions at the A1 and B1 direct excitonic transitions. PL spectra, as shown in Fig. 3c, were acquired on the same films used for Raman analysis. The PL intensity is normalised to the MoS_2 Raman signal in each case. The 5 nm film shows no PL, further implying that it constitutes bulk material. However, both the 0.5 nm and 1 nm films display the PL emissions characteristic of few layer crystals. These spectra were all acquired under identical acquisition conditions and so the high spectral intensity and, relative high intensity of the A1 to B1 emission observed for the 0.5 nm film imply that it is, at least partially, monolayer in nature. Six separate films with a starting thickness of 0.5 nm were fabricated and each one showed similar PL behaviour, indicating good reproducibility.

Scanning Raman spectroscopy was employed to assess the uniformity of a MoS_2 film over a large area. An optical image and Raman maps of a shadow mask patterned sample, with a starting Mo thickness of 10 nm, are shown in Fig. 3d. These demonstrate good uniformity in the film, with no cracks or tears observed over the scan area. Additionally, no MoS_2 is seen outside of the patterned region, signifying good control over feature placement when using shadow masks. Additional Raman maps, highlighting the increase in and A_{1g} peak separation with increasing thickness are shown in Fig. S2. Scanning Raman spectroscopy also allowed for PL spectra to be acquired over a large area. A PL surface map of a MoS_2 film, with a starting Mo thickness of 0.5 nm, is shown in Fig. S3. This shows a reasonably consistent signal, over a large area, further implying film uniformity, even in the case of very thin films. To the best of our knowledge, such uniform PL has not previously been reported for MoS_2 films produced by sulfurisation of Mo.

XPS measurements provided further information about the composition, purity and thickness of our films. They were performed on films which were produced from nominal Mo thicknesses of 0.5, 1 and 5 nm, sputtered onto Si/SiO_2 substrates, as well as on a clean Si/SiO_2 surface as a reference for film thickness estimation. An XPS survey spectrum of a MoS_2 film with a starting Mo thickness of 1 nm is shown in Fig. 4a. Aside from a weak carbon signal, which is generally unavoidable, no other contaminants were observed, indicating the high purity of our samples. In a previous XPS study on bulk MoS_2, Baker et al. show that the difference in binding energy between the Mo $3d_{5/2}$ and the S $2p_{3/2}$ peaks can be related to the stoichiometric composition of the MoS_2 [55]. All measured samples showed a ΔE value of 67.1 eV, corresponding to a stoichiometric ratio of $x = 1.9 \pm 0.1$. This is closer to the nominal value of 2 for MoS_2 than values reported previously for films produced by sulfurisation of MoS_2 (2.2) [31]. Furthermore, as shown in Fig. 4b, the Mo 3d core-level can be fitted with one main component at a binding energy of 230 eV for the Mo $3d_{5/2}$ peak, which originates from sulfurised Mo, and two smaller components on the high binding energy side of the peak which are most likely related to residual oxides. The S 2p core-level (not shown)

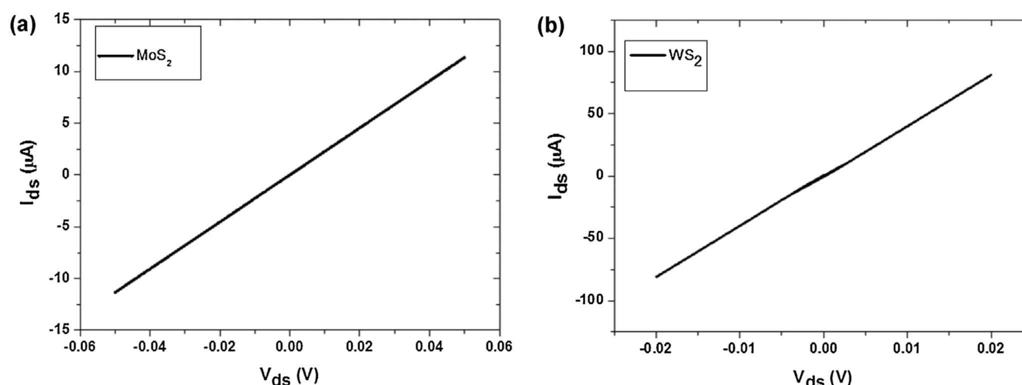

Fig. 7. (a) Current voltage characteristic of a MoS_2 device. The linear fit shows that ohmic contact was achieved between the MoS_2 and the sputtered contacts. Schottky effects are negligible due to work function match between Ti and MoS_2. (b) (I_{ds}–V_{ds}) plot of a WS_2 device. The linear fit shows that ohmic contact was also achieved between the WS_2 and the sputtered contacts.

Please cite this article in press as: R. Gatensby, et al., Controlled synthesis of transition metal dichalcogenide thin films for electronic applications, Appl. Surf. Sci. (2014), http://dx.doi.org/10.1016/j.apsusc.2014.01.103

could be fitted with only one component at a binding energy of 162.9 eV, indicating that there is no unreacted sulfur on the surface.

By comparing the areas of the silicon XPS peaks before and after growth of MoS_2 films on the Si/SiO_2 substrates, and using the exponential decay relation of photoelectrons emitted through an overlayer, the film thicknesses of different samples were estimated. The average thickness of a film with an initial nominal Mo thickness of 0.5 nm was found to be 2.0 nm. This corresponds to ~2–3 layers, given a typical MoS_2 interlayer thickness of 0.66 nm [31]. Similarly, films with starting thicknesses of 1 nm and 5 nm were measured to be 3.9 nm (6–7 layers) and 6.1 nm (9–10 layers) following sulfurisation. This is an expected result, as the film will expand upon the addition of S between the Mo layers. These estimated values are in close agreement with the Raman and PL observation which suggest thickness close to a monolayer. This expansion was also observed by atomic force microscopy, as shown in Fig. S4.

WS_2 films were also produced and characterised, demonstrating the flexibility of our production method. Raman spectra of such films are similar to those of MoS_2, with peaks corresponding to and A_{1g} vibrational modes. These are observed at 354 cm^{-1} and 420 cm^{-1}, respectively, as shown in Fig. 5a, which is in good agreement with literature values [56]. XPS analysis of the W 4f core-level, as shown in Fig. 5b, shows only one component at a binding energy of 33.05 eV (for the W $4f_{7/2}$) corresponding to sulfurised W with no indication of oxides being present on the surface. Similarly to the previously discussed MoS_2 samples, the survey scan shows no major contaminants and the S 2p core-level could only be fitted with one component at 162.5 eV (both not shown).

Devices were fabricated using selective area deposition, employing a shadow mask during the metal deposition, to create TMD patterns. A second shadow mask was used to pattern metal contacts on the thus derived films. A schematic of this is shown in Fig. 6. The bottom right panel in Fig. 6 is a photograph of such a device. Contacts were formed by sputtering Ti/Au (10/80 nm). The Ti serves two purposes, it acts as an adhesion layer for the gold, and it more closely matches the work function of the MoS_2, thereby limiting the height of the contact resistance at the interface. An interdigitated electrode (IDE) pattern, with a channel length of 200 μm and a width of 5.54 cm (=277 × Length) was used. Additional electrical measurements are included in the supporting information Figs. S6 and S7.

The source-drain current versus source-drain voltage (I_{ds}–V_{ds}) characteristic, for a pre-deposited Mo thickness of 20 nm, is shown in Fig. 7a. The 20 nm MoS_2 film is linear at a bias voltage sweep in the range of ±50 mV. The observed behaviour indicates that our device has intimate contact electrodes, with no contribution from a Schottky contact at the interface, thus excluding the possibility of a Schottky barrier, which would suppress charge carrier flow in the semiconducting channel. WS_2 devices exhibit the same ohmic (I_{ds}–V_{ds}) characteristic, as evidenced by the linear nature of Fig. 7b. The devices exhibit minimal contact resistance.

Fig. 8a shows typical gas sensor response curves of such a device at various concentrations of NH_3, from 400 ppb to 200 ppm. NH_3 is an electron-donating moiety and our sensor devices show n-type behaviour, thus adding majority carriers has the effect of increasing conductivity. A recent study on the gas sensing properties of mechanically exfoliated MoS_2 flakes illustrated a selective response to electron donors [47]. When the MoS_2 film is exposed to gaseous NH_3, adsorbed molecules on the surface of MoS_2 shift the Fermi level to the conduction band, resulting in the observed resistance decrease. Although the sensor response curves immediately indicate NH_3 injections, even at sub-ppm levels (Fig. 8b), recovery is slow in pure N_2 flow at room temperature; and baselines gradually shift downward for consecutive NH_3 injections. The surface may exhibit tight bonding with NH_3 molecules, as has commonly been

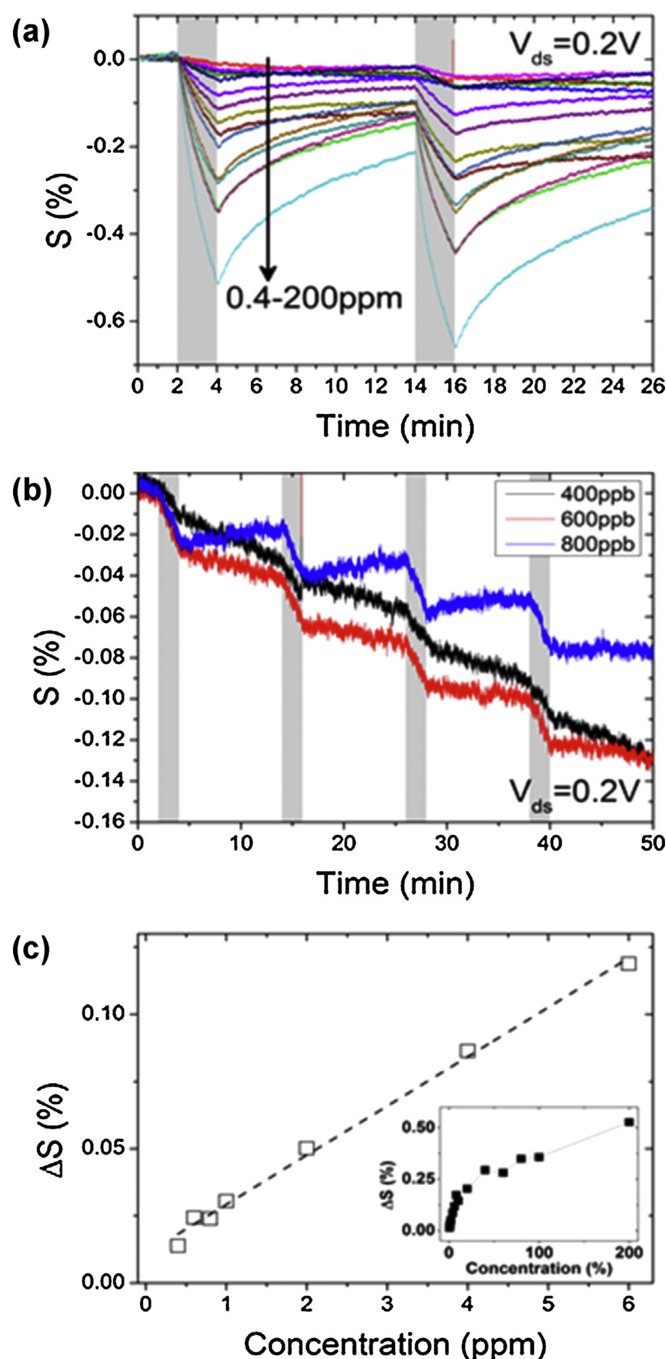

Fig. 8. (a) Sensor response (S) curves of the MoS_2 film at various NH_3 concentrations from 400 ppb to 200 ppm and (b) four-fold plots of sensor response at 400, 600, and 800 ppb. Grey vertical bars indicate NH_3 gas injections for 2 min. (c) Plots of sensitivity indicating percentile resistance changes between initial resistance and peak value of the first gas sensing cycle. Open boxes and broken line indicate measured data and fitted line, respectively. Inset: A full-scale sensitivity plot from 400 ppb to 200 ppm.

observed for nanomaterial-based sensors with extremely high sensitivities. The recovery speed could potentially be accelerated by ultra-violet illumination or annealing [43,57].

Sensor responses for ammonia gas injections, over 2 min intervals, define the sensor sensitivity in this study, as shown in Fig. 8c. In this study, sensor response (S) is defined by percentile resistance change, given by the following relation;

$$S = \frac{\Delta R}{R_0} = \frac{R_S - R_0}{R_0} \times 100\%$$

where R_0 is the initial resistance of the sensor and R_s is the resistance at gas introduction. The introduction of ammonia causes a decrease in S because $R_s < R_0$; therefore S is a negative quantity. The sensor sensitivity is linearly proportional to the concentration of NH_3 introduced in the low concentration range, which makes determination of gas concentration feasible, and a full-scale plot shows a hyperbolic curve (inset Fig. 8c). As a result, we obtained a practical detection limit of 400 ppb, which could be proven by signal-to-noise ratios (SNRs) based on simple signal processing. From the first 4000 data points (about 2 min), the initial resistance and root-mean-square (rms) noise of sensors were derived using the following equation;

$$\mathrm{rms}_{\mathrm{Noise}} = \sqrt{\frac{\sum(R - R_0)}{N}}$$

where R is the measured resistance and N is the number of data points. According to the IUPAC definition [58], the signal should be at least three times larger than the rms noise. Our MoS_2 sensors have a SNR of 8.3 at 400 ppb, and the SNR increases with increasing NH_3 concentration. Overall, this sensor performance is superior to previous reports on MoS_2 based ammonia sensors, produced from liquid phase exfoliated flakes, which show poor recovery at higher concentrations [50]. This low detection limit signifies that our MoS_2 sensor is a strong candidate for gas sensing applications. Functionalisation of the channel could engender selectivity in our device, as has been observed previously for other nanomaterial based sensors [44–46]. Sensors such as this, whereby a particular analyte (*e.g.* H_2S, CO_2) is targeted, are of high commercial interest.

4. Conclusion

We have shown a versatile method for the production of devices from TMD films, in particular with MoS_2 and WS_2. Control over film thickness was attained by modifying the thickness of pre-deposited metal layers. HRTEM studies outlined the crystalline quality of our samples with an FFT representative of hexagonal symmetry. XPS analysis further emphasised the high quality of the films, with minimal impurities present. The thinnest MoS_2 films (0.5 nm) exhibited a photoluminescence signal and Raman spectra, consistent with few-layer material. Films with starting thicknesses of 5 nm and greater displayed bulk like properties. These films were readily integrated into devices using a facile shadow masking procedure. Gas sensor devices produced in this manner display excellent sensitivity, with a detection limit of 400 ppb for ammonia. The ease of device manufacture, cost effectiveness, scalability and compatibility with existing semiconductor fabrication methods make this process favourable for future sensors and other electronic applications.

Acknowledgements

The authors thank Science Foundation Ireland (SFI) for financial support under Contract Nos. 08/CE/I1432 and PI_10/IN.1/I3030.

Appendix A. Supplementary data

Supplementary data associated with this article can be found, in the online version, at http://dx.doi.org/10.1016/j.apsusc.2014.01.103.

References

[1] Q.H. Wang, K. Kalantar-Zadeh, A. Kis, J.N. Coleman, M.S. Strano, Electronics and optoelectronics of two-dimensional transition metal dichalcogenides, Nat. Nanotechnol. 7 (2012) 699–712.
[2] M. Chhowalla, H.S. Shin, G. Eda, L.J. Li, K.P. Loh, H. Zhang, The chemistry of two-dimensional layered transition metal dichalcogenide nanosheets, Nat. Chem. 5 (2013) 263–275.
[3] X. Huang, Z. Zeng, H. Zhang, Metal dichalcogenide nanosheets: preparation, properties and applications, Chem. Soc. Rev. 42 (2013) 1934–1946.
[4] J.A. Wilson, A.D. Yoffe, The transition metal dichalcogenides discussion and interpretation of the observed optical, electrical and structural properties, Adv. Phys. 18 (1969) 193–335.
[5] A. Splendiani, L. Sun, Y. Zhang, T. Li, J. Kim, C.-Y. Chim, G. Galli, F. Wang, Emerging photoluminescence in monolayer MoS_2, Nano Lett. 10 (2010) 1271–1275.
[6] W.J. Zhao, Z. Ghorannevis, L.Q. Chu, M.L. Toh, C. Kloc, P.H. Tan, G. Eda, Evolution of electronic structure in atomically thin sheets of WS_2 and WSe_2, ACS Nano 7 (2013) 791–797.
[7] A. Ramasubramaniam, Large excitonic effects in monolayers of molybdenum and tungsten dichalcogenides, Phys. Rev. B 86 (2012).
[8] A. Kuc, N. Zibouche, T. Heine, Influence of quantum confinement on the electronic structure of the transition metal sulfide TS_2, Phys. Rev. B 83 (2011).
[9] K.K. Kam, B.A. Parkinson, Detailed photocurrent spectroscopy of the semiconducting Group-Vi transition-metal dichalcogenides, J. Phys. Chem.: US 86 (1982) 463–467.
[10] S.-W. Min, H.S. Lee, H.J. Choi, M.K. Park, T. Nam, H. Kim, S. Ryu, S. Im, Nanosheet thickness-modulated MoS_2 dielectric property evidenced by field-effect transistor performance, Nanoscale 5 (2013) 548.
[11] H. Li, Z. Yin, Q. He, H. Li, X. Huang, G. Lu, D.W.H. Fam, A.I.Y. Tok, Q. Zhang, H. Zhang, Layered nanomaterials fabrication of single- and multilayer MoS_2 film-based field-effect transistors for sensing NO at room temperature, Small 8 (2012) 63–67.
[12] H. Liu, J.J. Gu, P.D. Ye, MoS_2 nanoribbon transistors: transition from depletion mode to enhancement mode by channel-width trimming, IEEE Electron Dev. Lett. 33 (2012) 1273–1275.
[13] G. Eda, H. Yamaguchi, D. Voiry, T. Fujita, M. Chen, M. Chhowalla, Photoluminescence from chemically exfoliated MoS_2, Nano Lett. 11 (2011) 5111–5116.
[14] R.S. Sundaram, M. Engel, A. Lombardo, R. Krupke, A.C. Ferrari, P. Avouris, M. Steiner, Electroluminescence in single layer MoS_2, Nano Lett. 13 (2013) 1416–1421.
[15] J.N. Coleman, M. Lotya, A. O'Neill, S.D. Bergin, P.J. King, U. Khan, K. Young, A. Gaucher, S. De, R.J. Smith, I.V. Shvets, S.K. Arora, G. Stanton, H.-Y. Kim, K. Lee, G.T. Kim, G.S. Duesberg, T. Hallam, J.J. Boland, J.J. Wang, J.F. Donegan, J.C. Grunlan, G. Moriarty, A. Shmeliov, R.J. Nicholls, J.M. Perkins, E.M. Grieveson, K. Theuwissen, D.W. McComb, P.D. Nellist, V. Nicolosi, Two-dimensional nanosheets produced by liquid exfoliation of layered materials, Science 331 (2011) 568–571.
[16] R.J. Smith, P.J. King, M. Lotya, C. Wirtz, U. Khan, S. De, A. O'Neill, G.S. Duesberg, J.C. Grunlan, G. Moriarty, J. Chen, J. Wang, A.I. Minett, V. Nicolosi, J.N. Coleman, Large-scale exfoliation of inorganic layered compounds in aqueous surfactant solutions, Adv. Mater. 23 (2011) 3944–3948.
[17] Z. Zeng, T. Sun, J. Zhu, X. Huang, Z. Yin, G. Lu, Z. Fan, Q. Yan, H.H. Hng, H. Zhang, An effective method for the fabrication of few-layer-thick inorganic nanosheets, Angew. Chem. Int. Ed. 51 (2012) 9052–9056.
[18] Z. Zeng, Z. Yin, X. Huang, H. Li, Q. He, G. Lu, F. Boey, H. Zhang, Single-layer semiconducting nanosheets: high-yield preparation and device fabrication, Angew. Chem. Int. Ed. 50 (2011) 11093–11097.
[19] T. Drescher, F. Niefind, W. Bensch, W. Grünert, Sulfide catalysis without coordinatively unsaturated sites: hydrogenation, cis–trans isomerization, and H_2/D_2 scrambling over MoS_2 and WS_2, J. Am. Chem. Soc. 134 (2012) 18896–18899.
[20] G. Cunningham, M. Lotya, N. McEvoy, G.S. Duesberg, P. van der Schoot, J.N. Coleman, Percolation scaling in composites of exfoliated MoS_2 filled with nanotubes and graphene, Nanoscale 4 (2012) 6260.
[21] X. Huang, Z.Y. Zeng, S.Y. Bao, M.F. Wang, X.Y. Qi, Z.X. Fan, H. Zhang, Solution-phase epitaxial growth of noble metal nanostructures on dispersible single-layer molybdenum disulfide nanosheets, Nat. Commun. 4 (2013) (article no. 1444).
[22] Z. Zeng, C. Tan, X. Huang, S. Bao, H. Zhang, Growth of noble metal nanoparticles on single-layer TiS_2 and TaS_2 nanosheets for hydrogen evolution reaction, Energy Environ. Sci. (2014), http://dx.doi.org/10.1039/C1033EE42620C (advance article).
[23] W.J. Zhou, Z.Y. Yin, Y.P. Du, X. Huang, Z.Y. Zeng, Z.X. Fan, H. Liu, J.Y. Wang, H. Zhang, Synthesis of few-layer MoS_2 nanosheet-coated TiO_2 nanobelt heterostructures for enhanced photocatalytic activities, Small 9 (2013) 140–147.
[24] K. Chang, W. Chen, Single-layer MoS_2/graphene dispersed in amorphous carbon: towards high electrochemical performances in rechargeable lithium ion batteries, J. Mater. Chem. 21 (2011) 17175–17184.
[25] X. Cao, Y. Shi, W. Shi, X. Rui, Q. Yan, J. Kong, H. Zhang, Preparation of MoS_2-coated three-dimensional graphene networks for high-performance anode material in lithium-ion batteries, Small 9 (2013) 3433–3438.
[26] L. Cao, S. Yang, W. Gao, Z. Liu, Y. Gong, L. Ma, G. Shi, S. Lei, Y. Zhang, S. Zhang, R. Vajtai, P.M. Ajayan, Direct laser-patterned micro-supercapacitors from paintable MoS_2 films, Small (2013), http://dx.doi.org/10.1002/smll.201203164.
[27] S. Kumar, N. Peltekis, K. Lee, H.-Y. Kim, G. Duesberg, Reliable processing of graphene using metal etchmasks, Nanoscale Res. Lett. 6 (2011) 390.
[28] S. Kumar, N. McEvoy, T. Lutz, G.P. Keeley, V. Nicolosi, C.P. Murray, W.J. Blau, G.S. Duesberg, Gas phase controlled deposition of high quality large-area graphene films, Chem. Commun. 46 (2010) 1422–1424.
[29] X. Li, W. Cai, J. An, S. Kim, J. Nah, D. Yang, R. Piner, A. Velamakanni, I. Jung, E. Tutuc, S.K. Banerjee, L. Colombo, R.S. Ruoff, Large-area synthesis of high-quality and uniform graphene films on copper foils, Science 324 (2009) 1312–1314.

[30] D. Kong, H. Wang, J.J. Cha, M. Pasta, K.J. Koski, J. Yao, Y. Cui, Synthesis of MoS_2 and $MoSe_2$ films with vertically aligned layers, Nano Lett. 13 (2013) 1341–1347.
[31] Y. Zhan, Z. Liu, S. Najmaei, P.M. Ajayan, J. Lou, Large-area vapor-phase growth and characterization of MoS_2 atomic layers on a SiO_2 substrate, Small 8 (2012) 966–971.
[32] M.R. Laskar, L. Ma, S. Kannappan, P. Sung Park, S. Krishnamoorthy, D.N. Nath, W. Lu, Y. Wu, S. Rajan, Large area single crystal (0001) oriented MoS_2, Appl. Phys. Lett. 102 (2013).
[33] Y.-H. Lee, L. Yu, H. Wang, W. Fang, X. Ling, Y. Shi, C.-T. Lin, J.-K. Huang, M.-T. Chang, C.-S. Chang, M. Dresselhaus, T. Palacios, L.-J. Li, J. Kong, Synthesis and transfer of single-layer transition metal disulfides on diverse surfaces, Nano Lett. (2013) 130329103804007.
[34] Y.-H. Lee, X.-Q. Zhang, W. Zhang, M.-T. Chang, C.-T. Lin, K.-D. Chang, Y.-C. Yu, J.T.-W. Wang, C.-S. Chang, L.-J. Li, T.-W. Lin, Synthesis of large-area MoS_2 atomic layers with chemical vapor deposition, Adv. Mater. 24 (2012) 2320–2325.
[35] J. Mann, D. Sun, Q. Ma, J.-R. Chen, E. Preciado, T. Ohta, B. Diaconescu, K. Yamaguchi, T. Tran, M. Wurch, K. Magnone, T.F. Heinz, G.L. Kellogg, R. Kawakami, L. Bartels, Facile growth of monolayer MoS_2 film areas on SiO_2, Eur. Phys. J. B 86 (2013) 1–4.
[36] S. Najmaei, Z. Liu, W. Zhou, X. Zou, G. Shi, S. Lei, B.I. Yakobson, J.C. Idrobo, P.M. Ajayan, J. Lou, Vapour phase growth and grain boundary structure of molybdenum disulphide atomic layers, Nat. Mater. 12 (2013) 754–759.
[37] W.Y. Lee, T.M. Besmann, M.W. Stott, Preparation of MoS_2 thin-films by chemical vapor deposition, J. Mater. Res. 9 (1994) 1474–1483.
[38] K.-K. Liu, W. Zhang, Y.-H. Lee, Y.-C. Lin, M.-T. Chang, C.-Y. Su, C.-S. Chang, H. Li, Y. Shi, H. Zhang, C.-S. Lai, L.-J. Li, Growth of large-area and highly crystalline MoS_2 thin layers on insulating substrates, Nano Lett. 12 (2012) 1538–1544.
[39] M. Shanmugam, T. Bansal, C.A. Durcan, B. Yu, Schottky-barrier solar cell based on layered semiconductor tungsten disulfide nanofilm, Appl. Phys. Lett. 101 (2012) 263902–263905.
[40] T.W. Scharf, S.V. Prasad, M.T. Dugger, P.G. Kotula, R.S. Goeke, R.K. Grubbs, Growth, structure, and tribological behavior of atomic layer-deposited tungsten disulphide solid lubricant coatings with applications to MEMS, Acta Mater. 54 (2006) 4731–4743.
[41] J. Kong, N.R. Franklin, C.W. Zhou, M.G. Chapline, S. Peng, K.J. Cho, H.J. Dai, Nanotube molecular wires as chemical sensors, Science 287 (2000) 622–625.
[42] H. Li, Z.Y. Yin, Q.Y. He, X. Huang, G. Lu, D.W.H. Fam, A.I.Y. Tok, Q. Zhang, H. Zhang, Fabrication of single- and multilayer MoS_2 film-based field-effect transistors for sensing NO at room temperature, Small 8 (2012) 63–67.
[43] F. Schedin, A.K. Geim, S.V. Morozov, E.W. Hill, P. Blake, M.I. Katsnelson, K.S. Novoselov, Detection of individual gas molecules adsorbed on graphene, Nat. Mater. 6 (2007) 652–655.
[44] D.R. Kauffman, A. Star, Carbon nanotube gas and vapor sensors, Angew. Chem. Int. Ed. 47 (2008) 6550–6570.
[45] K.R. Ratinac, W.R. Yang, S.P. Ringer, F. Braet, Toward ubiquitous environmental gas sensors-capitalizing on the promise of graphene, Environ. Sci. Technol. 44 (2010) 1167–1176.
[46] T. Zhang, S. Mubeen, N.V. Myung, M.A. Deshusses, Recent progress in carbon nanotube-based gas sensors, Nanotechnology 19 (2008).
[47] F.K. Perkins, A.L. Friedman, E. Cobas, P.M. Campbell, G.G. Jernigan, B.T. Jonker, Chemical vapor sensing with monolayer MoS_2, Nano Lett. 13 (2013) 668–673.
[48] D.J. Late, Y.-K. Huang, B. Liu, J. Acharya, S.N. Shirodkar, J. Luo, A. Yan, D. Charles, U.V. Waghmare, V.P. Dravid, C.N.R. Rao, Sensing behavior of atomically thin-layered MoS_2 transistors, ACS Nano 7 (2013) 4879–4891.
[49] Q. He, Z. Zeng, Z. Yin, H. Li, S. Wu, X. Huang, H. Zhang, Fabrication of flexible MoS_2 thin-film transistor arrays for practical gas-sensing applications, Small 8 (2012) 2994–2999.
[50] Y. Yao, Z. Lin, Z. Li, X. Song, K.-S. Moon, C.-p. Wong, Large-scale production of two-dimensional nanosheets, J. Mater. Chem. 22 (2012) 13494–13499.
[51] K. Lee, R. Gatensby, N. McEvoy, T. Hallam, G.S. Duesberg, High performance sensors based on molybdenum disulfide thin films, Adv. Mater. 25 (2013) 6699–6702.
[52] M.M. Mdleleni, T. Hyeon, K.S. Suslick, Sonochemical synthesis of nanostructured molybdenum sulfide, J. Am. Chem. Soc. 120 (1998) 6189–6190.
[53] H. Li, Q. Zhang, C.C.R. Yap, B.K. Tay, T.H.T. Edwin, A. Olivier, D. Baillargeat, From bulk to monolayer MoS_2: evolution of raman scattering, Adv. Funct. Mater. 22 (2012) 1385–1390.
[54] A. Molina-Sánchez, L. Wirtz, Phonons in single-layer and few-layer MoS_2 and WS_2, Phys. Rev. B 84 (2011) 155413.
[55] M.A. Baker, R. Gilmore, C. Lenardi, W. Gissler, XPS investigation of preferential sputtering of S from MoS_2 and determination of MoS_x stoichiometry from Mo and S peak positions, Appl. Surf. Sci. 150 (1999) 255–262.
[56] J.W. Chung, Z.R. Dai, F.S. Ohuchi, WS2 thin films by metal organic chemical vapor deposition, J. Cryst. Growth 186 (1998) 137–150.
[57] J. Li, Y.J. Lu, Q. Ye, M. Cinke, J. Han, M. Meyyappan, Carbon nanotube sensors for gas and organic vapor detection, Nano Lett. 3 (2003) 929–933.
[58] L.A. Currie, Nomenclature in evaluation of analytical methods including detection and quantification capabilities (IUPAC Recommendations 1995), Pure Appl. Chem. 67 (1995) 1699–1723.

Please cite this article in press as: R. Gatensby, et al., Controlled synthesis of transition metal dichalcogenide thin films for electronic applications, Appl. Surf. Sci. (2014), http://dx.doi.org/10.1016/j.apsusc.2014.01.103